Desalination and Water Treatment
www.deswater.com

doi: 10.5004/dwt.2019.23695

149 (2019) 194–208
May

Preparation of hydroxyapatite biobased microcomposite film for selective removal of toxic dyes from wastewater

K. Azzaoui[a,*], E. Mejdoubi[a], A. Lamhamdi[a], M. Lakrat[a], O. Hamed[b,*], S. Jodeh[b], M. Berrabah[a], A. Elidrissi[c], I. El Meskini[d], M. Daoudi[d]

[a]*Laboratory of Mineral Solid and Analytical Chemistry (LMSAC), Department of Chemistry, Faculty of Sciences, Mohamed 1st University, P.O. Box 717, Oujda 60000, Morocco; Tel. +212 677042082; emails: k.azzaoui@yahoo.com (K. Azzaoui), ee.mejdoubi@gmail.com (E. Mejdoubi), abdellatiflamhamdi@hotmail.com (A. Lamhamdi), meddlakratl@gmail.com (M. Lakrat), berrabah.mohamed@laposte.net (M. Berrabah)*
[b]*Department of Chemistry, An-Najah National University, P.O. Box 7, Nablus, Palestinian Authority, Tel. +970594466271; emails: ohamed@najah.edu (O. Hamed), sjodeh@najah.edu (S. Jodeh)*
[c]*Laboratory LCAE-URAC18, Faculty of Sciences, Mohamed 1st University, Oujda 60000, Morocco, email: ab.elidrissi@yahoo.fr*
[d]*Laboratorie de Chimie Organique, Faculté des Sciences Dhar Mehraz, 30000 Fès, Morocco, emails: zouirchi2010@yahoo.fr (I. El Meskini), daoudimaria@yahoo.fr (M. Daoudi)*

Received 24 July 2018; Accepted 27 December 2018

ABSTRACT

The present work focused on designing and preparing a nature-based composite in film form to be used as an adsorbent for toxic dyes from wastewater. The composite film was prepared by a double decomposition and coprecipitation methods using hydroxyapatite (HAp), hydroxyethyl cellulose (HEC), and polyethylene glycol (PEG)-1000. Several films with various proportions were prepared. HEC used in this study was prepared from cellulose extracted from the natural plant Sparta "*Stipa tenacissima*" that is grown in the eastern region of Morocco. Prepared composite films were water insoluble, smooth, and flexible. The films were characterized by attenuated total reflectance infrared spectroscopy, thermal gravimetric analysis (differential thermal analysis), field emission scanning electron microscopy, and X-ray diffraction. The tendencies of the films for adsorbing methyl orange (MO) from water were evaluated. The film adsorption efficiencies were monitored by ultraviolet spectroscopy. Experimental data were described by Langmuir and Freundlich isotherm models. Results showed that the equilibrium data of MO adsorption were best represented by Freundlich isotherm model. The kinetic data of MO fitted well with the pseudo-second-order kinetic model. The results demonstrated that HAp/HEC/PEG composite achieved favorable removal of the toxic dye MO from water. The high efficiency of the composite toward MO could be related to the multi-coordination sites available on the film surface, the H-bonding sites, and the availability of macro tunnels in the composite structure. The antibacterial activities of several films were evaluated against gram-positive and gram-negative bacteria; all tested samples showed moderate to good activities. The results suggest that the composite of this study could be used as a potential low-cost alternative for removal of toxic dyes and bacteria from industrial wastewater.

Keywords: Hydroxyapatite; Biocompatibility; Composite; Methyl orange; Hydroxyethyl cellulose; Waste stream

* Corresponding authors.

1. Introduction

Water pollution is one of the major and most urgent issues of the modern world [1–3]. The major part of the pollution is generated by the industries. It is generated in two forms, smoke which causes air pollution and waste stream which causes ground water pollution. The waste stream composed of toxic metals in addition to organic matters. Among the organic matters that are produced and released in the waste stream are toxic dyes. The colored waste stream was generated mainly by textile mills. Recent reports published in *Bioresources Technology* [4] show that about one million dyes with different structures are available for commercial application, and about 100 million t/y of these dyes are released into the waste stream [1,4,5]. Most of these dyes are highly toxic, carcinogenic, and mutagenic; they are also known to cause irreversible damage to the environment. Their presence in the rivers and lakes destroy the food source of aquatic organisms by blocking the photosynthetic activities of aquatic flora. Therefore, the removal of these dyes from industrial waste streams is becoming a priority. Among these dyes, the most widely used is methyl orange (MO). It is used on a commercial scale despite its toxicity and carcinogenicity [6–10]. Therefore, it is necessary that this dye is removed from waste stream before it is discharged to the sewage system. Various methods for removal of MO from the waste stream are known and reported in the literature. Examples on these include adsorption [11–14], filtration [2], chemical oxidation [15], membrane biological treatment [16], ion exchange [4,17], and others [4,14,18]. So far, the most widely used technique is the adsorption, since it is easy to operate and showed the highest removal efficiency at lowest cost. Unlimited number of materials were evaluated for this purpose such as chitosan [19], activated carbon [20], magnetic nanoparticles [21–23], and others [21,24–26]. Among the other materials that were evaluated for adsorption of dyes from water are hydroxyapatite (HAp)-based composites. Some of these composites included cellulose polymer [1,27,28].

Cellulose and its derivatives attracted the attention of many researches since they possess properties that made them useful in a wide range of applications. They are renewable, biodegradable, biocompatible, and available at relatively low cost. In addition, when cellulose or its derivatives are used along with HAp in a composite, they enhance the absorption efficiency and the biodegradation properties of the composites.

Among the most interesting composites of calcium phosphate are those with the macro- and nanoporous regions. These regions allow bone colonization and neovascularization to the heart of the biomaterial. The presence of these regions in addition to the presence of metals enhances the interfacing with other organic materials such as cellulose and allows forming composites with unique functionalities [25].

Despite some adsorbents demonstrated high efficiency in removing various dyes from aqueous phase, a need still exists for an adsorbent that is selective, safe, natural, and available at low cost.

The present study was aimed to design and synthesize a novel nature-based composite for removal of MO from aqueous solution. The two natural products hydroxyethyl cellulose (HEC) and HAp were chosen for this purpose. The two materials are safe, biodegradable, and available at low cost. HEC used in this work was prepared from cellulose powder extracted from the biomass esparto. It is one of the most abundant biomasses in Morocco [29]; it belongs to the Graminae family, native to Spain and North Africa. In these regions, esparto has been used since ancient times to prepare ropes and basketry due to their strength. In recent years, the most common utilization of esparto is in the production of pulp for high-quality lightweight paper [29,30]. In addition, esparto was used in the production of livestock food and as a fuel.

The target composite was prepared by the double decomposition and coprecipitation methods. The composite was characterized by various spectroscopic and analytical techniques. Batch adsorption experiments were performed to evaluate the adsorption efficiency of the composite toward MO. The effects of variables, such as adsorbent dosage, contact time, initial MO concentration, and temperature, on MO removal were evaluated. The adsorption kinetics and isotherms of MO removal by HAp/HEC/polyethylene glycol (PEG) adsorbent were investigated. The adsorption rates were evaluated by fitting the experimental data to the kinetic models pseudo-first and second order. Results showed that the developed composite is useful for quantitative adsorption of the MO from aqueous solution with high adsorption capacities in short period.

2. Experimental

2.1. Materials

All reagents and solvents used in this work were purchased from Aldrich and used as received without any further purification. The reagents include calcium nitrate tetrahydrate $Ca(NO_3)_2{\cdot}4H_2O$ (99%), ammonium hydrogen phosphate $(NH_4)_2{\cdot}HPO_4$ (99%), dimethylformamide and PEG-1000. Distilled water was used in all the experiments. Hydroxyethyl cellulose (HEC, DS=1.5) used in this work was prepared according to a published method [27].

2.2. Methods

Prepared composites were subjected to analysis by various spectroscopic and analytical methods. Infrared (IR) spectra of composites were recorded on a Shimadzu attenuated total reflectance (ATR) Fourier transform IR (FTIR) 300 series instrument (Shimadzu Scientific Instruments).

Composite surface morphology was observed by using Hitachi SU820 field emission scanning electron microscope (SEM). The SEM analysis was performed on samples coated with gold/palladium. X-Ray diffraction (XRD) pattern was recorded with XPERT-PRO diffractometer using Cu Kα radiation (λ = 1.5418 Å) over a 2θ range of 10°–80° at a scan rate of 2°/min.

2.3. Cellulose extraction from Esparto

The Esparto "*Stipa tenacissima*" raw material was collected from the Eastern Morocco region, dried at room temperature in the shade, and cut into small pieces. Then it was

ground using a Herzog mill. Composition analysis of oven-dried samples of ground Esparto (moisture content 8%) showed the presence of 43 wt.% cellulose, 17 wt.% lignin, 8 wt.% ashes, and 3 wt.% silica. Other constituents present are about 21% [29].

The cellulose was extracted from the Esparto crops according to a procedure reported by El Idrissi et al. with some modification [30].

2.3.1. Removal of the extractives

A sample of ground esparto (10.0 g) was suspended in distilled water in a 250-mL flask and placed in a bath of boiling temperature for 5 h. This mixture was cooled to room temperature and diluted with 60 mL of THF/EtOH (1:1 by weight). The suspension was stirred at 60°C for 24 h. The solid mass was collected by vaccum filtration and washed three times with ethanol. The extraction process was performed multiple times to ensure complete removal of extractives.

2.3.2. Acid wash

After complete removal of the extractable materials, the solid residue was suspended in an aqueous solution of acetic acid (80 wt.%) in the presence of small amount of nitric acid at 10 wt.% concentration. The mixture was placed in a bath of boiling water under stirring for 2 h. Distilled water (30 mL) was then added to the mixture, and produced cellulose was collected and washed with distilled water to neutral.

2.3.3. Cellulose bleaching

Cellulose produced from the acid wash was suspended in a solution of sodium hydroxide (8 wt.%) containing 1.0 wt.% hydrogen peroxide. The mixture was heated in a water bath at 60°C for 2 h, then filtered, washed with water, and then suspended in an aqueous solution of sodium hypochlorite (2.0 wt.%). The treatment with sodium hypochlorite was carried out at 40°C for 2 h. Produced cellulose was collected by suction filtration, washed several times with water, and dried at room temperature.

2.3.4. Molecular weight of extracted cellulose

The molecular weight of cellulose used in this work was determined by gel-permeation chromatography/high-performance liquid chromatography (GPC/HPLC) combination. The HPLC was 1260 infinity from Agilent. The GPC detectors were an 18-angle light-scattering detector DAWN® HELEOS® II (Wyatt Technology) and the Refractive Index detector Optilab® T-REX (Wyatt Technology). The mobile phase carrying the polymeric materials was passed through a set of three columns that are connected in a series; the columns are 3 × PLgel 10 μm MIXED-B, 300 mm × 7.5 mm (Agilent), that are placed in a thermostatted heating compartment at 25°C. The system was operated at 25°C with a flow rate of 1 mL/min. The injection volume was 100 μL, and the run time was 40 min. The mobile phase was 0.5 wt.% LiCl/DMAc.

Calibration was done using an HPLC-grade toluene. Normalization was carried out on-line (with the columns) with 30,000 g/mol polystyrene at 0.5016 g/mL in 0.5% LiCl/DMAc. A sample of cellulose was dissolved in a solution of 8 wt.% of LiCl/DMAc solution according to the published procedure [31] and subjected to GPC analysis for molecular weight determination. The weight average molecular weight Mw was about 227,000 Dalton, and the number average molecular weight Mn was 122.7. The polydispersity was 1.85, and the degree of polymerization (DP) was 748.

2.3.5. Preparation of HEC

Extracted cellulose was then converted to HEC following a method reported in the literature; in this method, cellulose was dissolved in an aqueous solution of NaOH (12 wt.%) and urea (6 wt.%) [32–34]. Produced alkaline cellulose was then reacted with ethylene oxide.

2.4. Composite synthesis

The composite was synthesized using the double decomposition and coprecipitation methods. A solution of $Ca(NO_3)_2{\cdot}4H_2O$ was prepared by dissolving 11.76 g in a 100.0 mL distilled water. An aqueous solution of HEC (30 mL) was added to it, followed by the addition of a known amount of PEG-1000 (10 wt.% of the total weight of the composite). The produced solution was mixed for 10 min, and then an aqueous solution of $(NH_4)_2HPO_4$ (4.06 g) in a 100.0 mL distilled water was added over a period of 30 min with stirring at room temperature. The stirring was continued for 24 h, and the solution was then casted into a Petri dish and heated at 60°C. After complete evaporation of water, a film of HEC/HAp/PEG-1000 was formed. A photo of the produced film is shown in Fig. 1. Several films with various proportions were prepared (Table 1) following the above procedure.

2.5. Preparation of MO solution

A stock solution of MO with a concertation of 100 ppm was prepared by dissolving 0.1 g of MO in 1 L of double-distilled water. Diluted solutions of desired concentration were obtained by further dilution.

2.6. Batch adsorption and analysis

A batch process was performed on MO adsorption by using composite C (Table 1). In this process, a 0.1 g of composite C (Table 1) was added to each set of solutions (100.0 mL) of MO with certain concentration. The solutions were agitated for a desired adsorption time (10–60 min). The residual MO was analyzed by taking a 5.0 mL sample of supernatant, filtering it through a 0.45 micron syringe filter, and subjecting it to ultraviolet (UV) analysis using a UV-Vis spectrophotometer (Perkin Elmer, Model 550S with a 1 cm path length) set at a maximum wavelength of 464 nm. The amount of the dye adsorbed on the adsorbent Q_e (mg/g) and adsorbent efficiency were estimated according to Eqs. (1) and (2).

$$R(\%) = \frac{C_0 - C_e}{C_0} \times 100 \quad (1)$$

Fig. 1. A representative photo of the film obtained from the three components HAp/HEC/PEG-1000.

Table 1
Reagent and ratios used in the composite preparation

	HEC (wt.%)	HAp (wt.%)	PEG (wt.%)	Water (mL)
A	30	60	10	60
B	40	50	10	60
C	20	70	10	60
D	10	80	10	60

$$Q_e = \frac{C_0 - C_e}{m} \times V \quad (2)$$

C_0 and C_e are the initial and equilibrium concentrations (ppm) of MO in solution, respectively, Q_e (ppm) is the equilibrium adsorption capacity, W is the weight of the adsorbent (mg), and V is the volume of the solution (L).

2.7. Antimicrobial properties of composites

The disc diffusion method for antimicrobial susceptibility testing was followed according to a standard method recommended by the World Health Organization and the French standard NF-U-47-107 AFNOR 2004 [35]. The stains used in this study consisted of three gram-positive and one gram-negative bacteria (*Bacillus subtilis*, *Escherichia coli*, *Micrococcus luteus*) and one Candida (*Candida albicans*).

3. Results and discussion

3.1. FTIR analysis

The FTIR spectra of HAp and HEC materials are overlaid in Fig. 2(a). The HAp spectrum shows a peak at 1,635 cm^{-1}, which could be attributed to the CO stretching vibration. The peak at 1,100–900 cm^{-1} is corresponding to the PO_4^{3-} groups, and the bands at 1,093, 1,036, and 962 cm^{-1} are attributed to the phosphate stretching vibration P–O. The peaks with stretching frequencies of 1,090, 1,050, and 962 cm^{-1} are characteristics of apatitic structure. The bands with the frequencies of 602, 565, and 472 cm^{-1} are characteristics of PO_4^{3-}; the peaks are attributed to the phosphate bending vibration O–P–O.

HEC spectrum exhibiting a broad medium band centered at 3,350 cm^{-1} corresponds to the OH stretching vibration; the bands between 2,930 and 2,980 cm^{-1} are characteristic of the CH bonds of cellulose and CH_2 of ethoxy substituent. The broad strong band at 1,010 cm^{-1} is also a characteristic of C–O alcohols and ethers of cellulose anhydroglucose repeat unit.

Overlaid FTIR spectra of the composites with various component ratios are shown in Fig. 2(b). Comparing the spectra of the composites with those shown in Fig. 2(a) of the composite components, it can be concluded that the physical interaction between composite components is present. Two noticeable changes occurred to the CO bond signals: as the amount of apatite present in the composite increased, the bond frequency decreased and the intensity increased. The bond frequency of CO shifted from 1,635 to 1,623 cm^{-1}. Same effect occurred with the OH of HEC; the stretching of O–H is shifted to a lower wave number with more broadening going from low percentage of HAp to a higher percentage.

The result confirms the presence of a strong interaction between HEC and HAp. The interaction specifically occurs between the HAp metals and the OH groups of HEC.

A schematic model explaining the modifications occurred to HAp surface in an aqueous medium of PEG-1000 and the possible interaction between the OH groups of HEC and Ca^{2+} of HAp are shown in Fig. 2(c).

3.2. XRD analysis

The XRD analysis was performed on three composites with various proportions of HEC and HAp; results are shown in Fig. 3. The XRD was taken after calcination of the composites at 900°C. The XRD spectra of HAp are also included in Fig. 3(c) (JCPDS no. 09-0432); it shows two intense peaks around 26° and 31.8° (002) and (211), respectively. The peaks designate the crystallinity of HAp. The spectra in Figs. 3(a) and (b) show that these compounds retained some of the apatite structure. The peak at 2θ angular region of 31.8° (the most intense peak) corresponds to the crystalline region (211) of HAp. The XRD spectra also show that the size of the crystallinity level is inversely proportional to the organic contents of the composites. For instance, the lattice planes of HAp at (200), (111), (300), (301), (131), etc. can be clearly seen in sample b, and then the intensity of the peaks decreases and broadens in sample a. The splitting of the broadened peaks in the 2θ angular region of approximately 31°–34° of composites (a) and (b) indicates the lowering in the crystallinity level. The XRD results confirm the presence of an interaction between the organic and the inorganic components of the composite as also indicated by the FTIR.

The crystallite sizes in the three composites were calculated according to equation of Debye–Scherrer [Eqs. (3) and (4)].

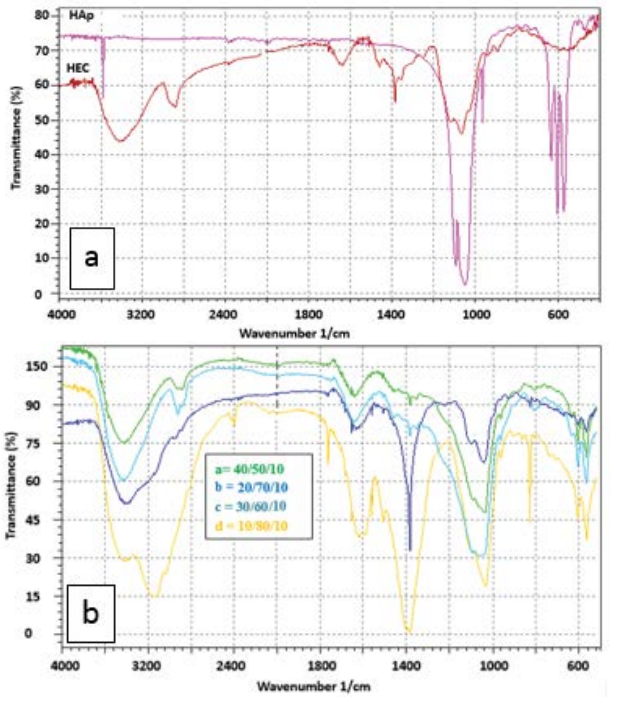

Fig. 2. FTIR spectra of (a) HEC, HAp, (b) HEC/HAp/PEG-1000 composites *a*, *b*, *c*, and *d*. (c) A schematic model shows the interaction between the OH groups of HEC and Ca^{2+} of hydroxyapatite.

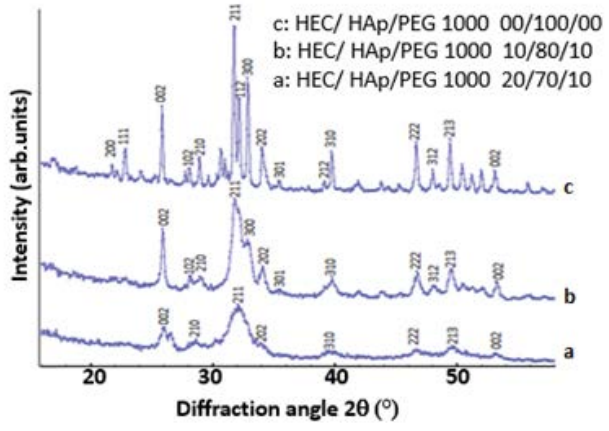

Fig. 3. XRD patterns of hydroxyapatite (HAp) and composites.

The peak broadening of XRD reflection was used to estimate the crystallite size in a direction perpendicular to the crystallographic plane based on Debye–Scherrer equation as follows [36]:

$$X_s = \frac{0.9\lambda}{\beta\cos\theta} \tag{3}$$

where X_s is the crystallite size (nm), λ is the wavelength of the X-ray beam (λ = 0.15406 nm for Cu Ka radiation), β is the full width at half maximum (FWHM) for the diffraction peak under consideration (rad), and θ is the diffraction angle. The diffraction peak at 26° was chosen for the calculation of crystallite size and crystallinity. The fraction of crystallinity X_c of the as-synthesized HAp/HEC/PEG composite was determined from the following equation [36]:

$$X_c = \left(\frac{0.24}{\beta}\right)^3 \tag{4}$$

where β is the FWHM.

Differential scanning calorimetry (DSC) analysis was performed on a DSC Q2000 V24.4 Build 116.

Prepared composite films were subjected to the total organic carbon (TOC) analysis (TOC/TN Analyzer multi N/C 2100/2100). Total carbon (TC) was used to represent the carbon content in an aqueous phase after suspension of the membrane in it. TC is preferred since it covers all carbon (organic and inorganic) existing in the aqueous effluent.

The results are summarized in Table 2. The diffraction peak at 25.5°–26° corresponding to (002) plane was selected for the calculation of crystallite size; it was isolated and sharp. The results demonstrate that sample with highest concentration of HEC exhibits poor crystallinity. The results are beneficial for biomedical purposes, since HAp with low crystallinity is needed due to their high in vivo resorbable property [1].

3.3. Thermal analysis of composites

Thermal analysis was performed on composites and starting materials. Thermogravimetric analysis coupled with the differential thermal analysis (TG/DTA) was performed at a temperature ranging from room to 1,000°C with a rise rate of 10°C/min.

The TG/DTA analytical curves of HEC, HAp, and composite are shown in Fig. 4. The TG/DTA curve of HEC shows three distinct stages. The first stage is between 25°C and 100°C, which could be related to the loss of water molecules. The second drop begins at about 165°C and ends at 262°C, which could be attributed to the decomposition of the side chains on the anhydroglucose repeat units of HEC. The third region occurred between 260°C and 400°C, which could be due to the cleavage of the cellulose glycosidic C–O linkage [37]. Complete decomposition of HEC repeat units started at about 361°C.

For composites A, B, C, and D, the decomposition temperatures were observed around 362°C, 366°C, 359°C, and 332°C, respectively, which demonstrated that the content of HEC must induce structural changes of HAp. As shown

Table 2
Crystallite size and crystallinity of HEC/HAp/PEG-1000 composite

Concentration of HEC	Plane	θ	FWHM (°)	Crystallite size, X_c (nm)	Crystallinity X_s (%)
0	002	12.94	0.3171	0.3435	4.4854
10	002	12.925	0.2672	0.7246	5.3219
20	002	12.915	0.2672	0.7250	5.3225

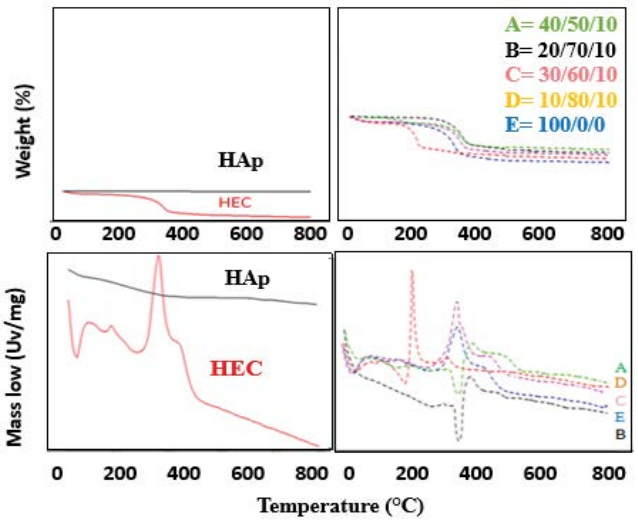

Fig. 4. Thermal gravimetric analysis/differential thermal analysis thermograms of HAp, HEC, and three composites of HEC/HAp/PEG-1000.

in the thermograms, the decomposition temperature of the composite films is slightly shifted to a higher temperature than that of the pure HEC, which again could be related to the interaction among composite components.

DSC thermograms of first and second scans of the composites C and D are shown in Fig. 5. The thermograms show two endothermic peaks, the first occurred at 100°C is attributed to the dehydration of HEC. The peak at 225°C is related to the endotherm fusion of HEC. The temperature of dehydration increased from 90.26°C to 94.67°C as the contents of HEC decreased from 20% to 10%. The same effect was seen with T_c and ΔH_f (Table 3).

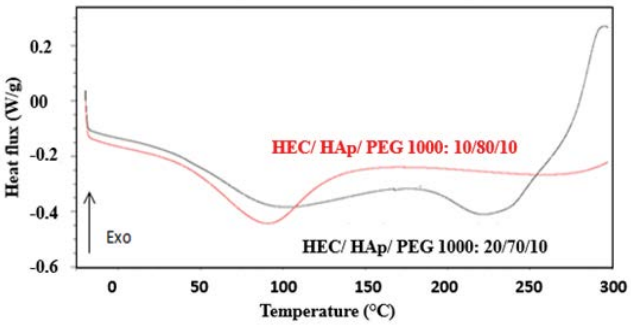

Fig. 5. DSC of composites C and D.

Table 3
The enthalpy values of composite obtained from the DSC scans

Composite-1000	ΔH_w (J/g)	T_c (°C)	ΔH_f (J/g)	T_m (°C)
C	55.38	94.67	33.29	225.74
D	78.16	90.26	14.44	256.29

ΔH_f: glass transition enthalpy, T_c: glass transition temperature, f: enthalpy or heat of fusion, and T_m: melting temperature.

3.4. Surface morphology

The SEM/FEG images of HAp and HAp/PEG-1000 are shown in Fig. 6(a). A pure sample of HAp that was sintered at 900°C for 2 h shows a platelet morphology. Images of HEC/HAp/PEG-1000 composite are shown in Fig. 6(b). All images show a surface that is composed of spherical particles like grains with a nanoscale size and macropores with dimensions ranging from 5 to 10 μm.

3.5. Antibacterial and antifungal test

The antimicrobial properties of the prepared tricomponent composites were evaluated against three bacterial stains and a fungus; results are summarized in Table 4. Antimicrobial reagent tetracycline was used as a control, which showed diameters of inhibition of 25–26 mm against gram-positive and 28 mm against gram-negative bacteria. The DMSO was used as a solvent; it showed no activities. Cycloheximide was also evaluated as a control; it showed a 26 mm diameter of inhibition against a fungus as shown in Fig. 7. Antimicrobial testing results are summarized in Table 5; all tested composites showed antifungal activities. The highest inhibition was found for composite B. The antimicrobial activity was selective for some composites; composite C showed only inhibition activity against *Bacillus*.

3.6. Adsorption of MO

3.6.1. Effect of contact time and concentration

The adsorption efficiencies of the composites for removal of MO from an aqueous solution as a function of temperature, contact time, composite concentration, and MO concentration were evaluated. Aqueous solutions of MO with various concentrations ranging from 3.27 to 32.35 ppm were subjected to adsorption by the composite B; all adsorption experiments were carried out at three different temperatures 289, 313, and 323 K; results are summarized in Fig. 8.

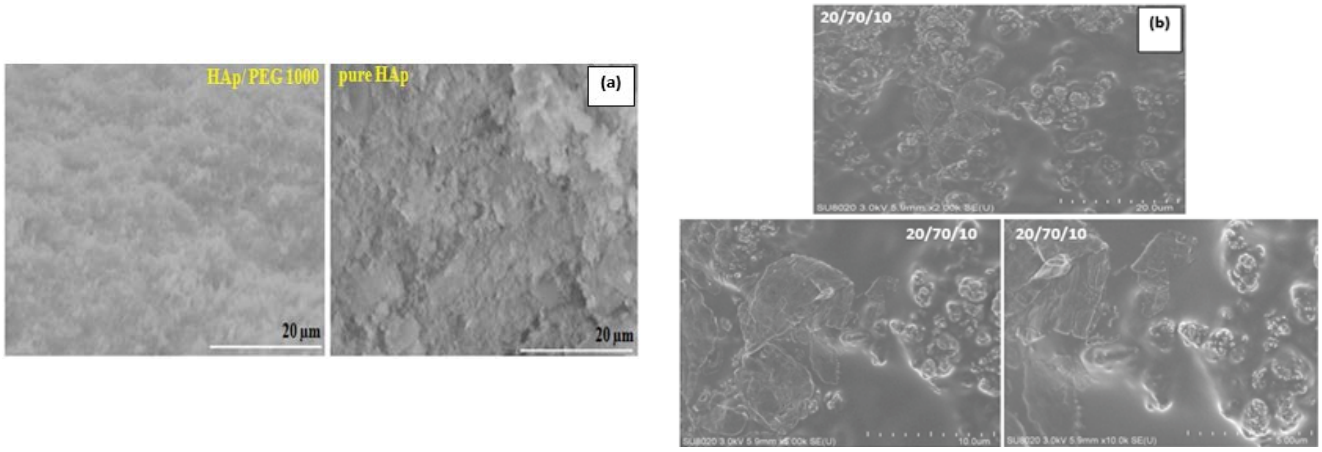

Fig. 6. (a) SEM/FEG images of HAp powder and a composite of HAp/PEG-1000 calcined at 900°C for 2 h and (b) SEM/FEG images of composite C.

Table 4
The diameter of inhibition of three composites with positive and negative control tested on three bacteria and one fungus

Stains	HEC/HAp/PEG 40/50/10	HEC/HAp/PEG 30/60/10	HEC/HAp/PEG 20/70/10	C+	DMSO
Bacillus subtilis	8	8	8	25	–
Micrococcus luteus	8	–	–	26	–
Escherichia coli	–	12	–	28	–
Candida	12	10	11	26	–

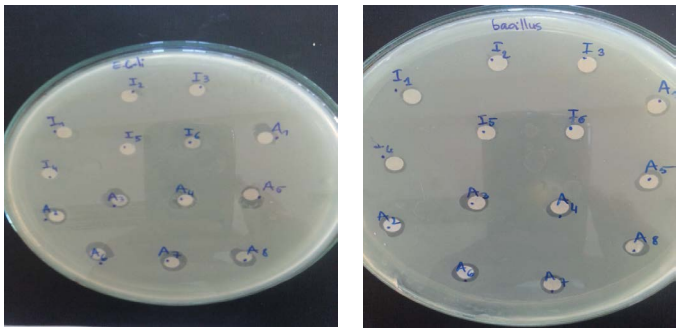

Fig. 7. Antimicrobial test results and sensitivity test in agar media.

Table 5
Langmuir and Freundlich parameters for the adsorption of MO onto HEC/HAp/PEG-1000 composite

T (K)		3.27			16.35			32.35		
C_0 (mg/L)		298	313	323	298	313	323	298	313	323
Langmuir isotherm	Q^0 (mg/g)	57.1428	135.135	112.3	98.03	181.81	142.8	156.25	90.00	125
	K_L (L/mg)	1.067	0.3894	0.689	0.085	0.04	0.144	0.0171	0.050	0.105
	R_L	0.227	0.4398	0.307	0.41	0.604	0.297	0.6429	0.377	0.226
	R^2	0.9718	0.9687	0.969	0.959	0.930	0.968	0.9238	0.968	0.994
Freundlich isotherm	$1/n$	0.8913	1.4805	1.095	1.094	1.356	1.611	1.9687	1.655	1.948
	K_F (L/mg)	17.135	15.235	23.56	3.045	1.908	4.631	0.0785	0.218	0.146
	R^2	0.6478	0.7707	0.716	0.698	0.882	0.531	0.776	0.597	0.571

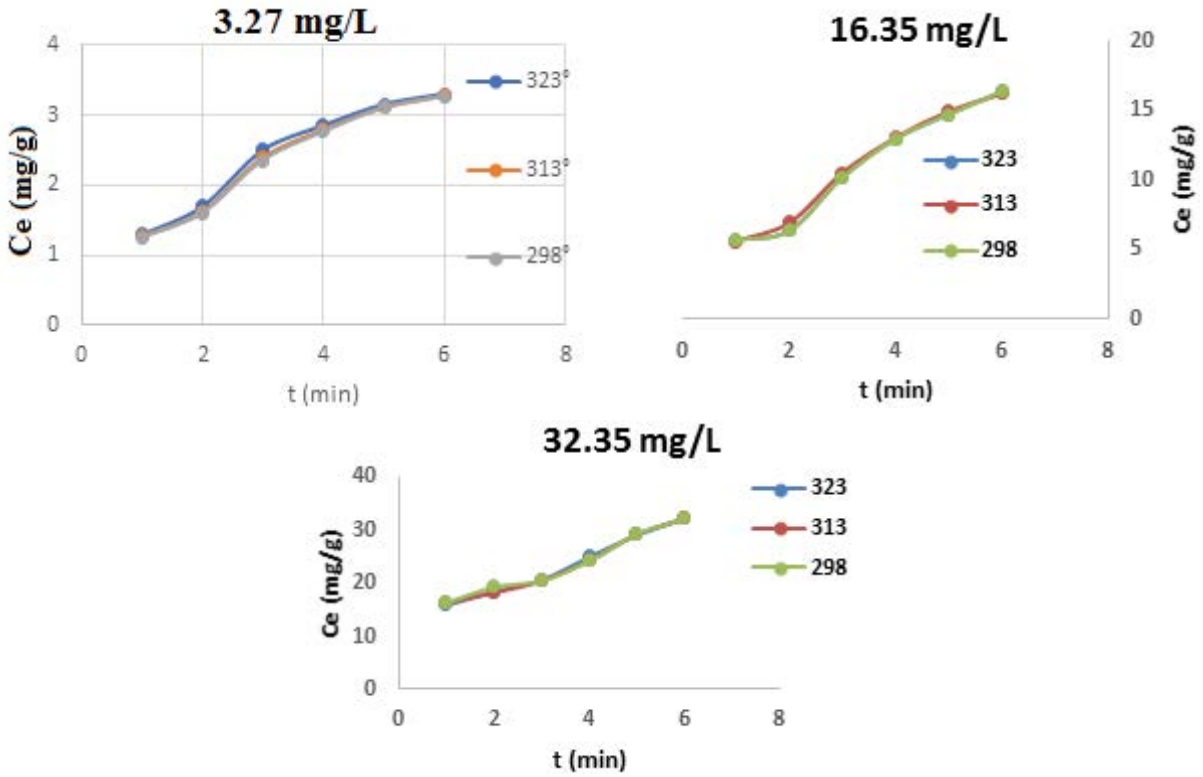

Fig. 8. Effect of contact time on the adsorption capacity of MO by the composite C at three different concentrations of MO.

As shown in Fig. 8, the adsorption started rapidly; it was almost complete in the first few minutes and then became much slower. The rapid adsorption at the initial contact time could be attributed to the plenty of the binding sites that are available on the surface of the composites, while the slow rate of MO adsorption was probably due to the electrostatic interaction between adsorbed and free molecules of MO.

Also Fig. 8 shows that the equilibrium adsorption capacity increased from 5 to 17 mg/g for composite B as the concentration of MO increased from 3 to 32 mg/L. This could be related to the fast diffusion of MO from the bulk solution to the composite surfaces as the concentration increases, which caused the equilibrium adsorption capacity to increase [38].

3.6.2. Impact of adsorbent dose on the extraction of MO

The effect of composite dose on the rate of MO adsorption from water was also evaluated; results are summarized in Fig. 9. As shown in Fig. 9, the rate of MO removal from water increased by increasing the amount of composite. The highest rate of adsorption was achieved at 323 K at a composite dose of 32.35 mg/L.

3.7. Adsorption isotherm

Adsorption isotherm models are important to investigate how adsorbates interact with adsorbents [27] and are widely used to describe the adsorption progress [10]. Two models Langmuir and Freundlich isotherms were used to study the adsorption equilibrium between the MO solution and the composite surface. The two isotherm models are important to determine the mode and the progress of interaction between adsorbent and adsorbate.

The two models Langmuir and Freundlich in Eqs. (5) and (6) [38].

Langmuir isotherm model

$$\frac{C_e}{Q_e} = \frac{1}{q_{\max}} C_e + \frac{1}{q_{\max} K_L} \tag{5}$$

where C_e is the equilibrium concentration of MO (ppm), Q_e is the amount of adsorbate adsorbed per unit mass of HEC/HAp/PEG-1000 composite at equilibrium (mg/g), $q_{\max}$ is the theoretical maximum monolayer adsorption capacity of the adsorbent (mg/g), and K_L is the Langmuir isotherm constant related to the adsorption energy (L/mg).

Freundlich isotherm model

$$\ln\left(Q_e\right) = \ln k_f + \frac{1}{n} \ln C_e \tag{6}$$

where K_F and $1/n$ are empirical constants that indicate the relative adsorption capacity and intensity related to the affinity of the metal, respectively [32].

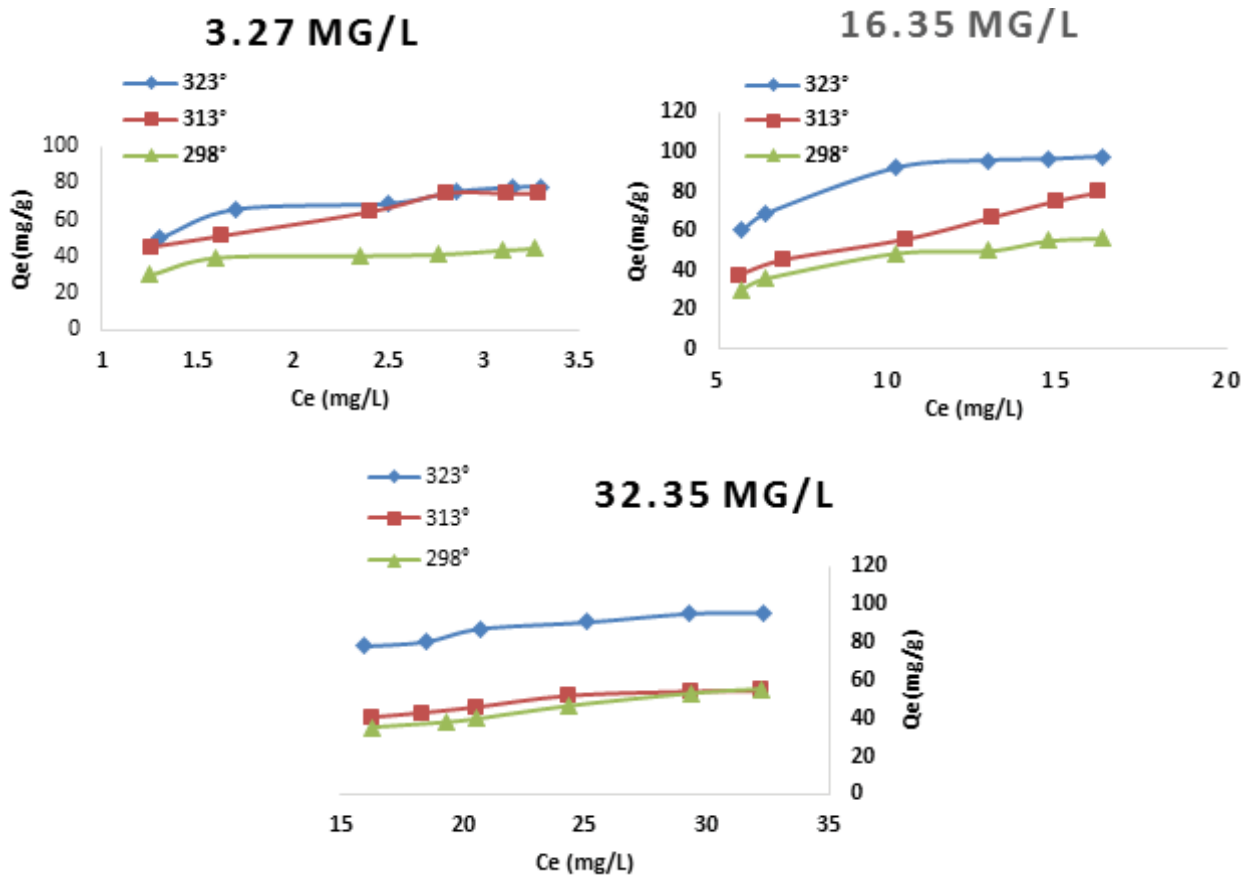

Fig. 9. Effect of adsorbent dosage on rate of adsorption of MO.

From Langmuir isotherm model, it could also be predicted if the adsorption is favorable or not using the dimensionless constant separation factor shown in Eq. (7).

$$R_L = \frac{1}{1 + K_L C_0} \tag{7}$$

where K_L is the Langmuir constant and C_0 is the initial adsorbate concentration. If R_L value is greater than 1, then the adsorption is unfavorable. But if the value is between 1 and 0, then the adsorption is favorable, and R_L = 1 means linear adsorption.

Freundlich isotherm [Eq. (8)] represents the nonideal adsorption that includes heterogeneous surface energy system.

$$Q_e = K_F C_e^{1/n} \tag{8}$$

where K_F (L/mg) is the Freundlich constant and 1/n is the adsorption intensity, and if 1/n is >0.1 and <0.5, then the adsorption is favorable, for 1/n value higher than 2 means unfavorable.

Table 5 and Figs. 10,11 and 12 summarize all fitting parameters; the correlation coefficients were greater than 0.99. The separation factor R_L which was calculated for various amounts of adsorbents of HEC/HAp/PEG-1000 composite was $0 < R_L < 1$. The 1/n value ranged from 0.8913 to 1.0955. The results indicate that the adsorption of MO by the composite follows Langmuir isotherm model (3), where the MO molecules are equally and homogeneously spread over the porous surfaces of the composite HEC/HAp/PEG-1000.

3.8. Kinetic adsorption of MO

Kinetic adsorption study is important to determine the type of adsorption mechanism involved in the adsorption process, since it could be a mass transfer or chemical bonding; the collected MO adsorption data were analyzed using the pseudo-first-order and pseudo-second-order kinetic models. The linearized forms of the rate equations [39] were estimated according to Eqs. (9)–(12).

$$\ln\left(q_e - q_t\right) = \ln q_e - K_1 t \tag{9}$$

$$\frac{t}{q_t} = \frac{1}{K_2 q_e^2} + \frac{t}{q_e} \tag{10}$$

$$Q_t = K_{id} t^{1/2} + Z \tag{11}$$

$$\ln\frac{K\left(T_2\right)}{K\left(T_1\right)} = \frac{E_a}{R}\left(\frac{1}{T_1} - \frac{1}{T_2}\right) \tag{12}$$

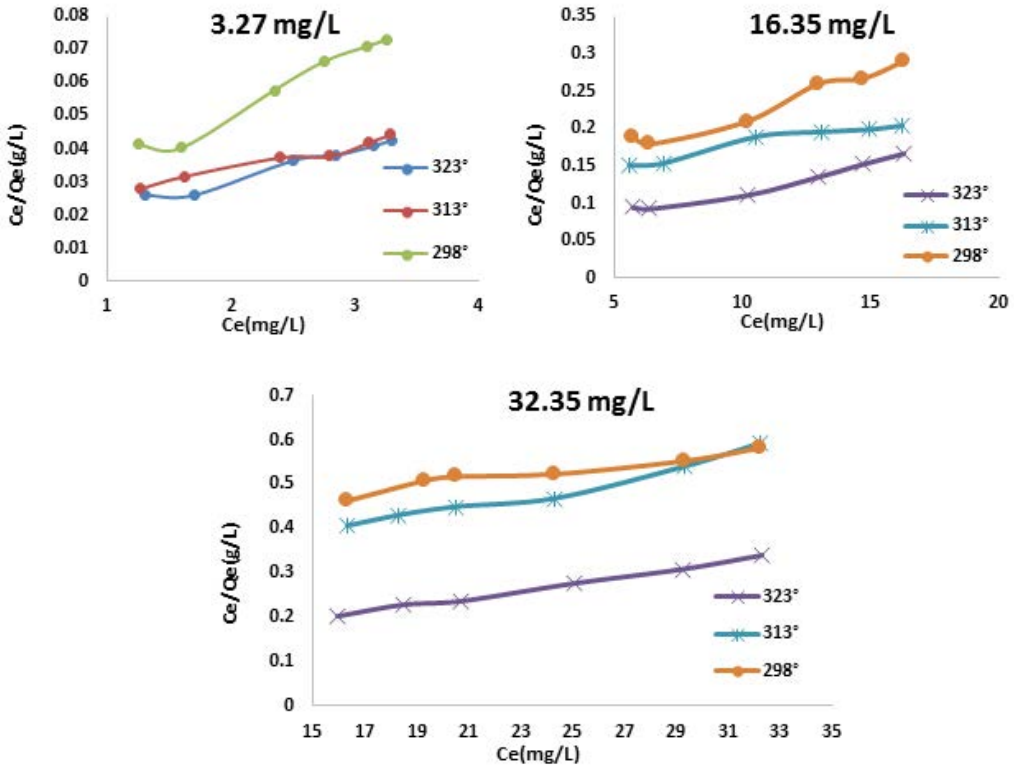

Fig. 10. Langmuir isotherm model for MO adsorption on HEC/HAp/PEG-1000 composite.

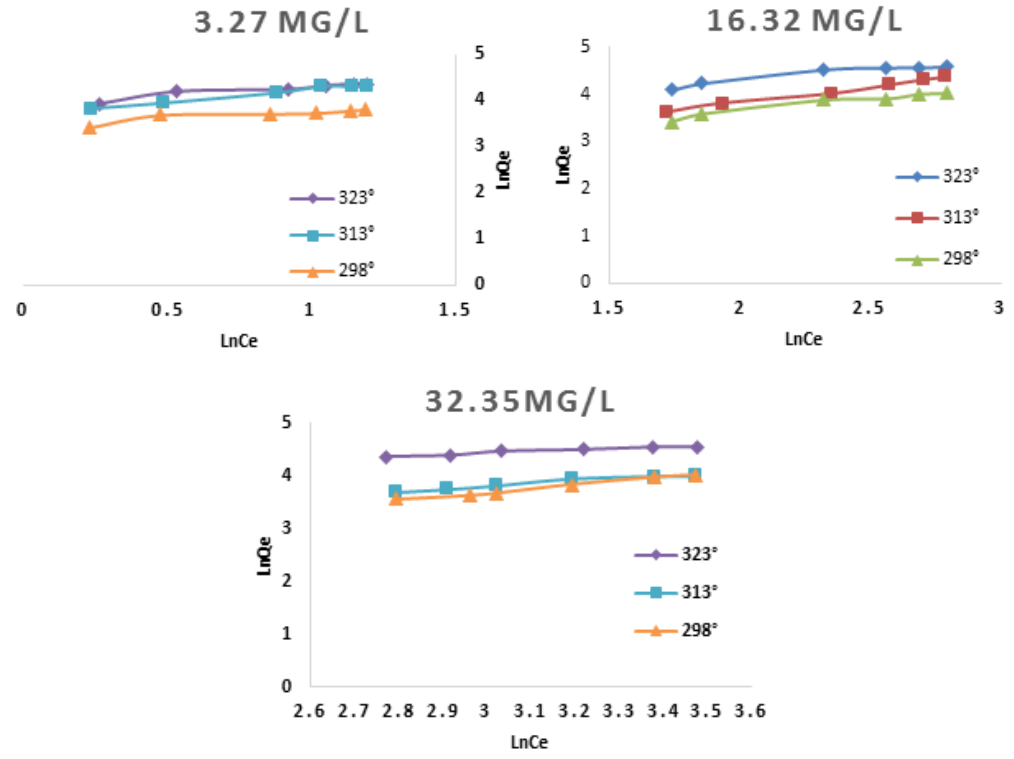

Fig. 11. Freundlich isotherm model for MO adsorption on HEC/HAp/ PEG-1000 composite.

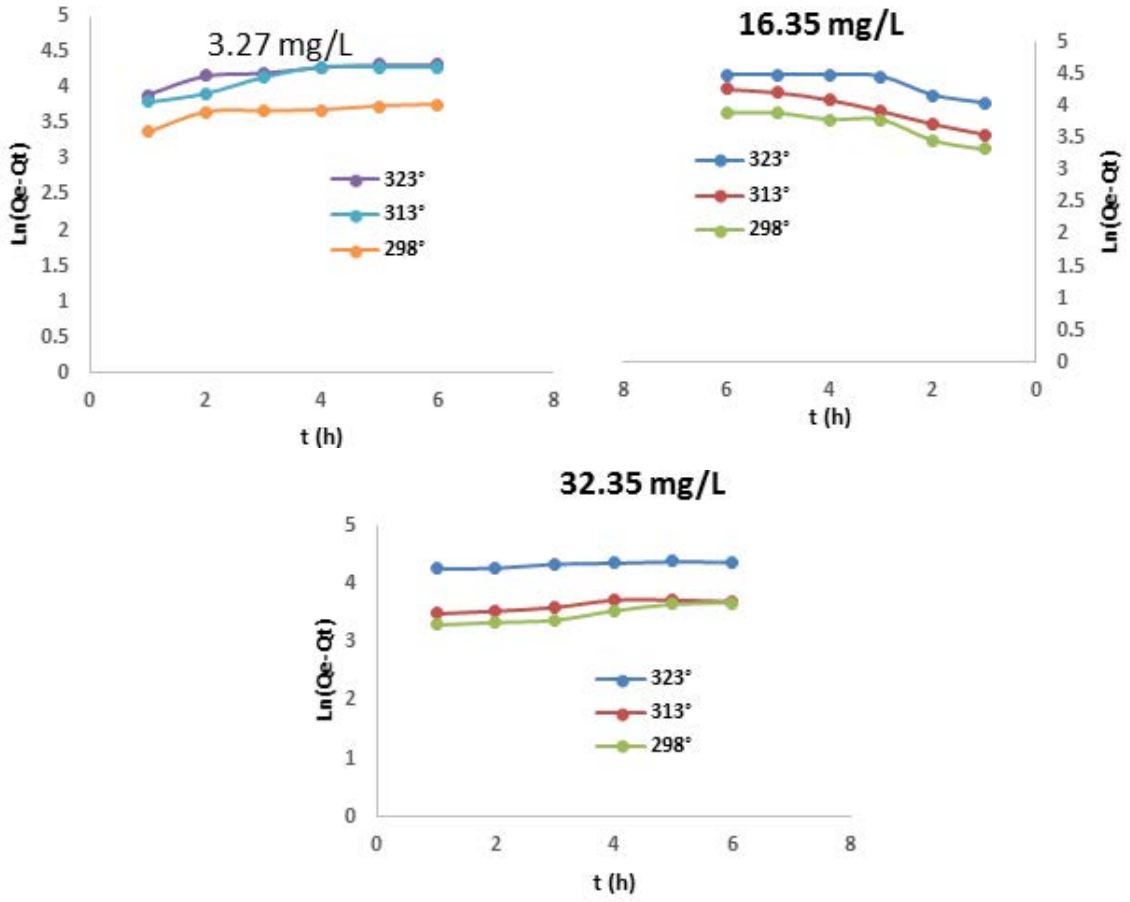

Fig. 12. Pseudo-first-order model for the adsorption of MO onto composite C.

where Q_e and Q_t are adsorption capacities (mg/g) at equilibrium and at various time (t, min). K_1 is the pseudo-first-order rate constant (/min), and K_2 is the pseudo-second-order rate constant (g/mg min). The K_{id} is the intraparticle diffusion rate constant (mg/g/min$^{1/2}$), and Z (mg/g) could be used to conclude the thickness of the boundary layer.

The Gibbs energy ($\Delta G°$), enthalpy ($\Delta H°$), and entropy ($\Delta S°$) were calculated according to the following equations:

$$K_c = \frac{C_{ads}}{C_e} \tag{13}$$

$$\Delta G^o = -RT \ln K_c \tag{14}$$

$$\ln K_s = \frac{\Delta S}{R} - \frac{\Delta H}{RT} \tag{15}$$

where K_c is an apparent constant of the thermodynamics; C_{ads} is the adsorbed amount at equilibrium, mg/L; C_e is the equilibrium concentration in the supernatant, mg/L; R is the universal gas constant, J/mol K; and T is the solution temperature, K.

The adsorption kinetics of MO on composite film C was studied at three different concentrations 3.27, 16.35, and 32.7 mg/L. The experimental data were fitted for pseudo-first and second order and the intraparticle diffusion model as shown in Eqs. (7)–(10) above [38]. The obtained values of the kinetic parameters are shown in Tables 6 and 7 and Figs. 12 and 13. When the experimental data were plotted for both the pseudo-first-order and the pseudo-second-order kinetics, the correlation coefficients (R^2) for the pseudo-second order were higher than that for pseudo-first order and it reached 1. The results agree with the theoretical values, which indicate that the adsorption process of MO on the surface of the HEC/HAp/PEG-1000 follows the pseudo-second order.

The values of K_{id} and Z were calculated from the graph obtained from Q_t vs. $t^{1/2}$ (Fig. 13). The values are shown in Table 8. All plots shown in Fig. 13 were linear and did not pass through the origin indicating the presence of more than one rate-limiting process.

The initial linearity of the graphs shown in Fig. 14 indicates that at the initial stage, the adsorption of MO by HEC/HAp/PEG-1000 composite occurred on the exterior surface. The other linearities in the graphs indicate a gradual adsorption of MO and an intraparticle diffusion rate-limiting step. Table 7 shows that the values of Z increase as the concentration of MO increases. This could be

Table 6
The pseudo-second-order model for adsorption of MO by HEC/HAp/PEG-1000 composite C

T (K)	298			313			323		
C_0 (mg/L)	K_2 (g/mg min)	Q_{cal} (mg/g)	R^2	K_2 (g/mg min))	Q_{cal} (mg/g)	R^2	K_2 (g/mg min))	Q_{cal} (mg/g)	R^2
3.27	0.1127	2.562	0.9219	0.0123	14.1242	0.962	0.02137	20.7468	0.9063
16.35	0.1073	2.4348	0.9441	0.01220	13.5501	0.9892	0.02177	19.0476	0.9
32.25	0.1009	2.8810	0.9593	0.01025	16.1290	0.9314	0.0203	20.7468	0.9063

Table 7
Parameters explain the intraparticle diffusion of MO into the composite structure

T (K)	298			313			323		
C_0 (mg/L)	K_{id}	Z	R^2	K_{id}	Z	R^2	K_{id}	Z	R²
3.27	0.7151	0.086	0.9693	3.5817	1.4367	0.9958	5.5137	1.8862	0.9309
16.35	0.6771	0.1358	0.9776	3.529	1.2557	0.9976	5.084	1.4027	0.9301
32.35	0.8385	0.1701	0.9554	4.0157	1.6892	0.9917	5.5137	1.8862	0.9309

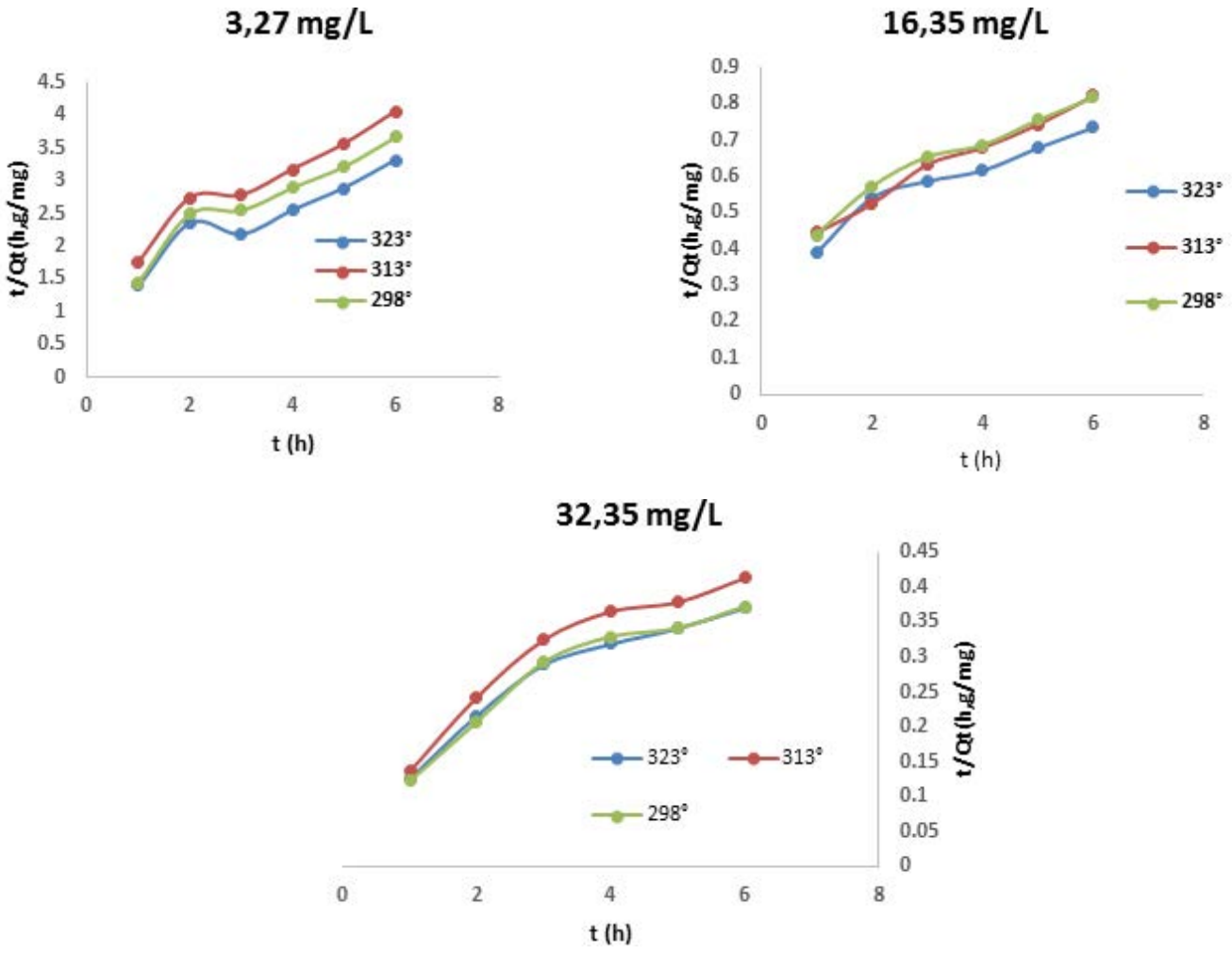

Fig. 13. Pseudo-second-order model for the adsorption of MO onto composite C.

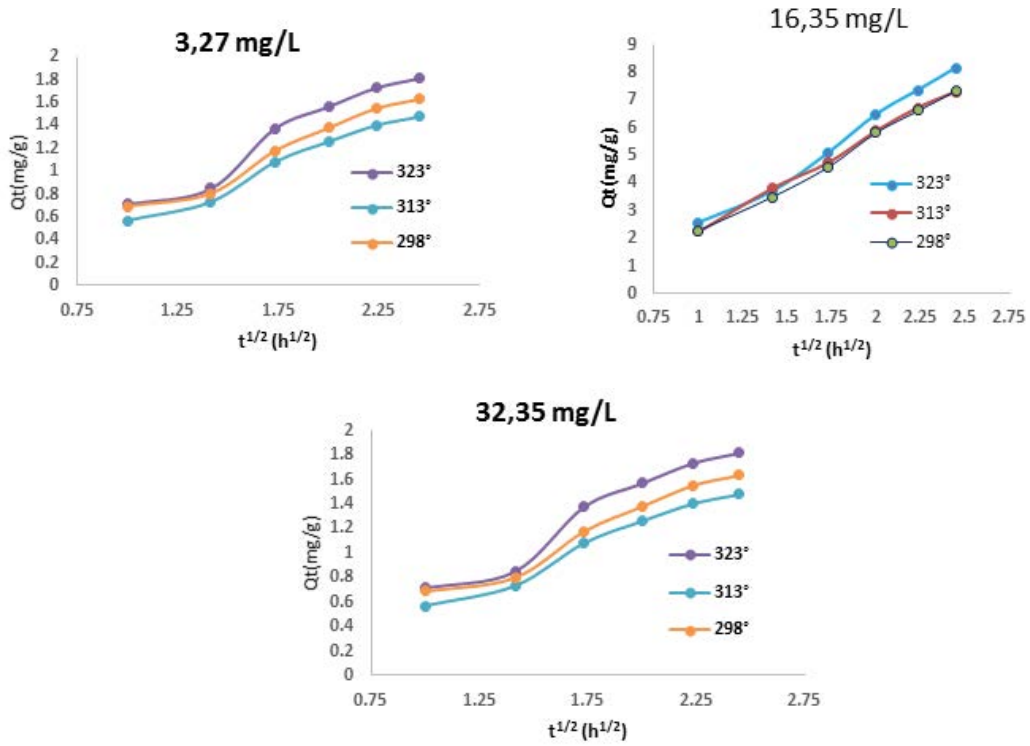

Fig. 14. Intraparticle diffusion model for the adsorption of MO onto composite C at various concentrations.

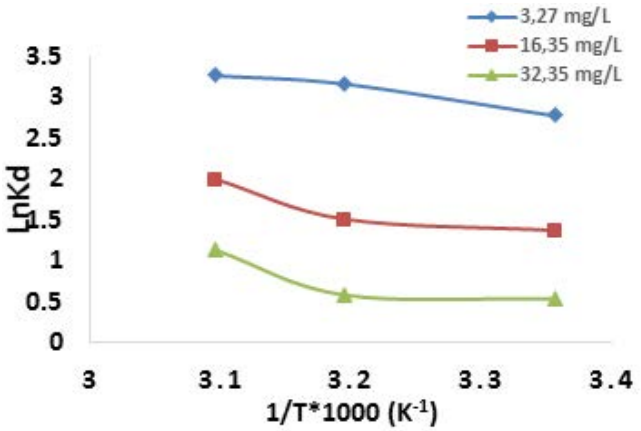

Fig. 15. Adsorption thermodynamics of MO onto composite C.

related to an expansion in the outer layer and dwindling in external mass transfer while the potential for internal mass transfer increased; we also noticed similar behavior in the previously published results [39].

The activation energy of the adsorption process was calculated at 298 and 323 K using Eq. (9). The value was close to zero, indicating a spontaneous adsorption process.

3.9. Adsorption thermodynamics

The thermodynamic behavior of adsorption of MO dye by the HEC/HAp/PEG-1000 composite was also evaluated. The thermodynamic parameters equilibrium rate constant (K) (L/g), the standard Gibbs free energy ($\Delta G°$) (J/mol), the standard entropy ($\Delta S°$) (J/mol/K), and the standard enthalpy ($\Delta H°$) (J/mol) were determined at various temperatures (K) using Van't Hoffs equation [Eq. (16)] [38]. The standard Gibbs free energy ($\Delta G°$) (J/mol) was calculated according to Eq. (17).

$$\ln K_s = \frac{\Delta S}{R} - \frac{\Delta H}{RT} \tag{16}$$

Table 8
Thermodynamic parameters for the adsorption of MO onto HAp composite

$C°$ (mg/L)	3.27 mg/L			16.35 mg/L			32.35 mg/L		
Temperature (K)	$\Delta G°$ (KJ/mol)	$\Delta H°$ (KJ/mol)	$\Delta S°$ (J/K mol)	$\Delta G°$ (KJ/mol)	$\Delta H°$ (KJ/mol)	$\Delta S°$ (J/K mol)	$\Delta G°$ (KJ/mol)	$\Delta H°$ (KJ/mol)	$\Delta S°$ (J/K mol)
298	–22.96	16.02	77.09	–21.99	18.76	73.85	–18.61	17.49	62.53
313	–24.11			–23.10			–19.55		
323	–24.89			–23.84			–20.17		

$$\Delta G^{o} = \Delta H^{o} - T\Delta S^{o} \quad (17)$$

The $\ln K_s$ vs. $1/T$ was plotted as shown in Fig. 15; the slopes and the intercept were used to calculate various thermodynamic parameters as shown in Table 8.

The obtained values of $\Delta S°$ and $\Delta H°$ were positive as shown in Table 8. The entropy increased at the solid/solution interface driven by the adsorption process, and the $\Delta H°$ values showed an endothermic nature of the HEC/HAp/PEG-1000 composite [36]. Also, from the results, it was found that free energies for all HEC/HAp/PEG-1000 composites were negative indicating a spontaneous adsorption process at different temperatures.

The spontaneous nature of the adsorption process could be attributed initially to the electrostatic interaction between HEC/HAp/PEG-1000 composite components and MO, which then leads to a complexation between the aromatic ring of the MO and the metal ions in the composite. Intermolecular forces including H bonding and dipole-dipole interaction between HEC and MO could be another reason for a spontaneous adsorption.

4. Conclusion

Nature-based tricomponent composites in film form were designed, synthesized, and evaluated as adsorbents for toxic dyes from water. The composites consist of HEC, HAp, and PEG-1000 that were mixed at various proportions. PEG-1000 was used as a diluent to enhance the interfacing between HAp and HEC. The prepared composites were subjected to analysis by ATR-FTIR, X-ray diffraction, SEM, and thermal analysis. The results revealed the existence of strong interactions between composite components. SEM images showed that the composites have smooth surfaces that are composed of spherical particles with a diameter of about 90 nm. The composites were evaluated in a microscale extraction process of MO from water. Extraction efficiencies of several composite films were monitored by UV spectrophotometer. The rate of adsorption showed some dependence on temperature, amount of adsorbent, and adsorbate. The adsorption mechanism was predicted by Langmuir isotherm model. Kinetic data revealed that the adsorption of MO obeys the pseudo-second order. Thermodynamic data showed free energies with negative values, indicating a spontaneous adsorption process of MO onto the composite surface.

Acknowledgements

The authors would like to thank Mohamed 1st University in Morocco and An-Najah National University in Palestine for the financial support of this work.

References

[1] K. Azzaoui, E. Mejdoubi, A. Lamhamdi, S. Zaoui, M. Berrabah, A. Elidrissi, B. Hammouti, M.M. Fouda, S.S. Al-Deyab, Carbohydr. Polym., 115 (2015) 170–176.
[2] M. Liu, Q. Chen, K. Lu, W. Huang, Z. Lü, C. Zhou, S. Yu, C. Gao, High efficient removal of dyes from aqueous solution through nanofiltration using diethanolamine-modified polyamide thin-film composite membrane, Sep. Purif. Technol., 173 (2017) 135–143.
[3] E. Alver, M. Bulut, A.Ü. Metin, H. Çiftçi, One step effective removal of Congo Red in chitosan nanoparticles by encapsulation, Spectrochim. Acta A Mol. Biomol. Spectrosc., 171 (2017) 132–138.
[4] T. Robinson, G. McMullan, R. Marchant, P. Nigam, Remediation of dyes in textile effluent: a critical review on current treatment technologies with a proposed alternative, Bioresour. Technol., 77 (2001) 247–255.
[5] M.T. Yagub, T.K. Sen, S. Afroze, H.M. Ang, Dye and its removal from aqueous solution by adsorption: a review, Adv. Colloid Interface Sci., 209 (2014) 172–184.
[6] U. Habiba, T.A. Siddique, T. Chin, A. Salleh, B. Chin, A.M. Afifi, Synthesis of chitosan/polyvinyl alcohol/zeolite composite for removal of methyl orange, Congo red and chromium (VI) by flocculation/adsorption, Carbohydr. Polym., 157 (2017) 1568–1576.
[7] Y. Qi, M. Yang, W. Xu, S. He, Y. Men, Natural polysaccharides-modified graphene oxide for adsorption of organic dyes from aqueous solutions, J. Colloid Interface Sci., 486 (2017) 84–96.
[8] R. Shan, L. Yan, Y. Yang, K. Yang, S. Yu, H. Yu, Highly efficient removal of three red dyes by adsorption onto Mg–Al-layered double hydroxide, J. Ind. Eng. Chem., 21 (2015) 561–568.
[9] C. Lei, M. Pi, P. Kuang, Y. Guo, F. Zhang, Organic dye removal from aqueous solutions by hierarchical calcined Ni-Fe layered double hydroxide: isotherm, kinetic and mechanism studies, J. Colloid Interface Sci., 496 (2017) 158–166.
[10] I.M. Arabatzis, T. Stergiopoulos, M.C. Bernard, D. Labou, S.G. Neophytides, P. Falaras, Silver-modified titanium dioxide thin films for efficient photodegradation of methyl orange, Appl. Catal. B, 42 (2003) 187–20.
[11] W. Yao, S. Yu, J. Wang, Y. Zou, S. Lu, Y. Ai, N.S. Alharbi, A. Alsaedi, T. Hayat, X. Wang, Enhanced removal ofmethyl orange on calcined glycerol-modified nanocrystallined Mg/Al layered double hydroxides, Chem. Eng. J., 307 (2017) 476–486.
[12] Ihsanullah, F.A. Al-Khaldi, B. Abusharkh, M. Khaled, M.A. Atieh, M.S. Nasser, T. Laoui, T.A. Saleh, S. Agarwal, I. Tyagi, V.K. Gupta, Adsorptive removal of cadmium(II) ions from liquid phase using acid modified carbon-based adsorbents, J. Mol. Liq., 204 (2015) 255–263.
[13] A. Abbas, B.A. Abussaud, N.A.H. Al-Baghli, Ihsanullah, M. Khraisheh, M.A. Atieh, Benzene removal by iron oxide nanoparticles decorated carbon nanotubes, J. Nanomater., (2016) 1–10.
[14] U. Habiba, T.A. Siddique, T. Chin, A. Salleh, B. Chin, A.M. Afifi, Carbohydr. Polym., 157 (2017) 1568–1576.
[15] L.L. Gershbein, Food Chem. Toxicol., 20 (1982) 1–8.
[16] K. Azzaoui, A. Lamhamdi, E. Mejdoubi, M. Berrabah, A. Elidrissi, B. Hammouti, J. Chem. Pharm. Res., 5 (2013) 1209–1216.
[17] C.H. Liu, J.S. Wu, H.C. Chiu, S.Y. Suen, K.H. Chu, Removal of anionic reactive dyes from water using anion exchange membranes as adsorbers, Water Res., 41 (2007) 1491–1500.
[18] K. Azzaoui, A. Lamhamdi, E. Mejdoubi, M. Berrabah, B. Hammouti, A. Elidrissi, M.M.G. Fouda, S.S. Al-Deyab, Carbohydr. Polym., 111 (2014) 41–46.
[19] M.S. Chiou, P.Y. Ho, H.Y. Li, Adsorption of anionic dyes in acid solutions using chemically cross-linked chitosan beads, Dyes Pigm., 60 (2004) 69–84.
[20] F. Rozada, L.F. Calvo, A.I. García, J. Martín-Villacorta, M. Otero, Dye adsorption by sewage sludge-based activated carbons in batch and fixed-bed systems, Bioresour. Technol., 87 (2003) 221–230.
[21] X. Wu, W. Wang, F. Li, S. Khaimanov, N. Tsidaeva, PEG-assisted hydrothermal synthesis of $CoFe_2O_4$ nanoparticles with enhanced selective adsorption properties for different dyes, Appl. Surf. Sci., 389 (2016) 1003–1011.
[22] R. Chen, W. Wang, X. Zhao, Y. Zhang, S. Wu, F. Li, Rapid hydrothermal synthesis of magnetic Cox Ni1 − x Fe_2O_4 nanoparticles and their application on removal of Congo red, Chem. Eng. J., 242 (2014) 226–233.
[23] X. Zhao, W. Wang, Y. Zhang, S. Wu, F. Li, J.P. Liu, Synthesis and characterization of gadolinium doped cobalt ferrite nanoparticles with enhanced adsorption capability for Congo Red, Chem. Eng. J., 250 (2014) 164–174.

[24] S.J. Allen, G. Mckay, J.F. Porter, Adsorption isotherm models for basic dye adsorption by peat in single and binary component systems, J. Colloid Interface Sci., 280 (2004) 322–333.
[25] O. Ozdemir, B. Armagan, M. Turan, M.S. Çelik, Comparison of the adsorption characteristics of azo-reactive dyes on mezoporous minerals, Dyes Pigm., 62 (2004) 49–60.
[26] M.R. Fathi, A. Asfaram, A. Farhangi, Removal of Direct Red 23 from aqueous solution using corn stalks: isotherms, kinetics and thermodynamic studies, Spectrochim. Acta A Mol. Biomol. Spectrosc., 135 (2015) 364–372.
[27] H. Zhang, Q. Luan, H. Tang, F. Huang, M. Zheng, Q. Deng, X. Xiang, C. Yang, J. Shi, C. Zheng, Q. Zhou, Removal of methyl orange from aqueous solutions by adsorption on cellulose hydrogel assisted with Fe_2O_3 nanoparticles, Cellulose, 24 (2017) 903–914.
[28] G. Annaduraia, R.-S. Juang, D.-J. Leea, Use of cellulose-based wastes for adsorption of dyes from aqueous solutions, J. Hazard. Mater., 92 (2002) 263–274.
[29] S. Belkhir, A. Koubaa, A. Khadhri, M. Ksontini, H. Nadji, S. Smiti, et al., Seasonal effect on the chemical composition of the leaves of *Stipa tenacissima* L. and implications for pulp properties, Ind. Crops Prod., 44 (2013) 56–61.
[30] S. El Barkany, A. El Idrissi, C. Zanagui, I. Jilal, F. Tabaght, M. Abou-Salama, H. Amhamdi, New branched chain cellulose derivatives based on Esparto "*Stipa tenacissima*" of eastern Morocco: synthesis and characterization, J. Mater. Environ. Sci., 8 (2017) 1195–1210.
[31] H. Yang, O. Hamed, R. Salghi, N. Abidi, S. Jodeh, R. Hattb, Extraction an characterization of cellulose from agricultural waste Argan Press Cake Cellulose, Chem. Technol., 51 (2017) 263–272.
[32] J.P. Zhou, L.N. Zhang, Polym. J., 32 (2000) 866.
[33] L. Wang, J. Zhang, R. Zhao, C. Li, Y. Li, C. Zhang, Desalination, 254 (2010) 68–74.
[34] Z. Qi, Z. Lina, L. Ming, W. Xiaojun, C. Gongzhen, J. Polym. Bull., (2005) 53–243.
[35] A.W. Bauer, W.M.M. Kirby, J.C. Serris, M. Turck, Antibiotic susceptibility testing by a standardized single disc method, Am. J. Clin. Pathol., 45 (1966) 493–496.
[36] K. Azzaoui, E. Mejdoubi, Faculty of Sciences, Thesis, Mohamed 1st University, Oujda, Morocco, 14 (2014) 286.
[37] X.-G. Li, M.-R. Huang, H. Bai, Thermal decomposition of cellulose ethers, J. Appl. Polym. Sci., 73 (1999) 2927–2936.
[38] S. Jodeh, J. Amarah, S. Radi, O. Hamed, I. Warad, R. Salghi, A. Chetouni, S. Samhan, R. Alkowni, J. Chem., 4 (2016) 140–156.
[39] K.A.G. Gusmão, L.V.A. Gurgel, T. Melo, L.F. Gil, Application of succinylated sugarcane bagasse as adsorbent to remove methylene blue and gentian violet from aqueous solutions – kinetic and equilibrium studies, Dyes Pigm., 92 (2012) 967–974.